Original Article

Bioprinting of three-dimensional dentin–pulp complex with local differentiation of human dental pulp stem cells

Journal of Tissue Engineering
Volume 10: 1–10

DOI: 10.1177/2041731419845849
journals.sagepub.com/home/tej
SAGE

Jonghyeuk Han[1], Da Sol Kim[2], Il Ho Jang[2,3], Hyung-Ryong Kim[4,5] and Hyun-Wook Kang[1]

Abstract

Numerous approaches have been introduced to regenerate artificial dental tissues. However, conventional approaches are limited when producing a construct with three-dimensional patient-specific shapes and compositions of heterogeneous dental tissue. In this research, bioprinting technology was applied to produce a three-dimensional dentin–pulp complex with patient-specific shapes by inducing localized differentiation of human dental pulp stem cells within a single structure. A fibrin-based bio-ink was designed for bioprinting with the human dental pulp stem cells. The effects of fibrinogen concentration within the bio-ink were investigated in terms of printability, human dental pulp stem cell compatibility, and differentiation. The results show that micro-patterns with human dental pulp stem cells could be achieved with more than 88% viability. Its odontogenic differentiation was also regulated according to the fibrinogen concentration. Based on these results, a dentin–pulp complex having patient-specific shape was produced by co-printing the human dental pulp stem cell–laden bio-inks with polycaprolactone, which is a bio-thermoplastic used for producing the overall shape. After culturing with differentiation medium for 15 days, localized differentiation of human dental pulp stem cells in the outer region of the three-dimensional cellular construct was successfully achieved with localized mineralization. This result demonstrates the possibility to produce patient-specific composite tissues for tooth tissue engineering using three-dimensional bioprinting technology.

Keywords

Bioprinting, stem cells, cell differentiation, dentin, dental pulp, tissue engineering

Date received: 19 March 2019; accepted: 2 April 2019

Introduction

In 2011–2012, approximately 52% of adults aged 20–64 years in the United States and approximately 158 million people worldwide suffered from severe tooth loss.[1,2] Non-biological (artificial) dental implants are the most commonly used therapy to treat such tooth loss. This approach has the advantage that it can rapidly recover tooth function with a natural appearance. However, differences in physical and physiological properties between the

[1]Biomedical Engineering, School of Life Sciences, Ulsan National Institute of Science and Technology (UNIST), Ulsan, South Korea
[2]Department of Oral Biochemistry, School of Dentistry, Pusan National University, Yangsan, South Korea
[3]Institute of Translational Dental Sciences, School of Dentistry, Pusan National University, Yangsan, South Korea
[4]Institute of Tissue Regeneration Engineering (ITREN), Dankook University, Cheonan, South Korea
[4]College of Dentistry, Dankook University, Cheonan, South Korea

Corresponding authors:
Hyung-Ryong Kim, Institute of Tissue Regeneration Engineering (ITREN), Dankook University, Cheonan, 31116, South Korea.
Email: hrkimdp@gmail.com

Hyun-Wook Kang, Biomedical Engineering, School of Life Sciences, Ulsan National Institute of Science and Technology (UNIST), 50, UNIST-gil, Ulsan 44919, South Korea.
Email: hkang@unist.ac.kr

dental implant and a human tooth frequently cause peri-implantitis with alveolar bone loss.[3,4] Approximately, 64% of donors underwent alveolar bone loss within 2 months of dental implant surgery.[5] In order to solve these problems, cell-based artificial teeth having similar physiological properties with real teeth have been considered as a new alternative to dental implants.

To date, numerous attempts have been made to develop cell-based artificial teeth confirming the possibility for artificial regeneration of teeth and the surrounding tissue, including alveolar bones and periodontal ligaments.[6–8] Studies with tooth germ have been frequently conducted, which was implanted into animals to study the subsequent tooth formation.[9–13] This method could induce the formation of composite tissues similar to a real tooth. Scaffold-based approaches were also introduced for artificial regeneration with tooth cells.[14,15] These approaches also successfully showed the possibility to produce tooth-shaped tissues. However, both attempts were not able to produce patient-specific shaped composite tissues composed of pulp, dentin, and enamel.[16–18] Structural and compositional similarities between real teeth and three-dimensional (3D) patient-specific shapes are crucial points for future clinical application. Tooth germ–based approaches had limitations in controlling the size and shape of the tooth and are difficult to culture primary biological sources for preparing the germ structures. In addition, scaffold-based approaches were not suitable for the regeneration of tooth-like composite tissues because this approach could not precisely place multiple types of cells in a pre-defined manner.

The 3D bioprinting technology provides a unique tool to overcome these difficulties. This method can produce 3D freeform cellular constructs using multiple types of living cells, biomolecules, and biomaterials.[19–21] It not only enables the regeneration of tooth-like composite tissues but can also precisely control the shape of the regenerated tissue using medical imaging data from the patient.[22–24] Despite these advantages of 3D bioprinting, to the best of our knowledge, no one has applied this technique to reconstruct patient-specific dental composite tissues.[25]

In this study, we investigated the possibility of regenerating patient-specific shaped and tooth-like composite tissue utilizing 3D bioprinting technology. A fibrin-based bio-ink was designed for 3D printing of human dental pulp stem cells (hDPSCs). The effects of fibrinogen concentration within the bio-ink were examined based on cytocompatibility, printability, and odontogenic differentiation. We also investigated the possibility of localized odontogenic differentiation of hDPSCs in a printed structure and applied this technology to construct a patient-specific shaped 3D dentin–pulp complex.

Materials and methods

Preparation of fibrin-based bio-ink

We designed a fibrin-based bio-ink composed of fibrinogen, gelatin, hyaluronic acid (HA), and glycerol (Sigma Aldrich Co., St. Louis, PA, USA) for hDPSC printing. For the preparation of bio-ink, HA was dissolved in a modified Eagle's Minimum Essential Medium (MEM; Gibco, Waltham, MA, USA) at a concentration of 3 mg/mL by gently rotating at 37°C overnight. Gelatin and fibrinogen were then dissolved into the HA solution at concentrations of 37.5 and 5–20 mg/mL, respectively. Finally, glycerol was mixed at a concentration of 4% v/v. Through this procedure, four bio-ink groups were prepared, which are F5-, F10-, F15-, and F20-bio-inks having fibrinogen concentrations of 5, 10, 15, and 20 mg/mL, respectively. The prepared bio-ink was sterile-filtered (0.45 pm filters) and stored at −20°C until used.

Cell culture and cell–laden bio-ink preparation

The hDPSCs (Lonza, Walkersville, MD, USA) were cultured with StemMACS™ Expansion Media XF (Miltenyi Biotec GmbH, Bergisch Gladbach, Germany) supplemented with 1% v/v penicillin-streptomycin (P/S) in physiological conditions (37°C, 5% CO_2). The medium was exchanged every 3 days. Subculturing was conducted at 70%–80% confluency by dissociation with TrypLE™ Select (1×) (Gibco). StemMACS OsteoDiff media (Miltenyi Biotec GmbH) containing 1% v/v P/S was used as odontogenic differentiation medium. In the culture of hDPSC-laden bio-ink, aprotinin (Sigma) was added to the culture medium at a concentration of 10 μg/mL in order to prevent excessive bio-ink degradation.

For the bioprinting process, harvested hDPSCs were mildly and homogeneously mixed with melted bio-ink at a desired concentration. The prepared hDPSC-laden bio-inks were loaded into 1-mL syringes and incubated in a 4°C refrigerator for 4 min to induce gelation. The bio-ink-laden syringes were connected to the micro-nozzle and installed into the dispensing module of the bioprinting system (Figure 1(a)).

3D bioprinting system

A hybrid bioprinting system, capable of printing biodegradable thermoplastics and cell-laden bio-inks simultaneously, was used to fabricate dentin–pulp complexes.[26] For this purpose, a custom 3D bioprinter was utilized, consisting of three-axis stages for motion control, multi-cartridge dispensing modules to deliver multiple types of cell and biomaterial, and an enclosure that can control temperature, humidity, and cleanliness (Figure 1(a)).

Bioprinting of 3D patient-specific tooth-shaped cellular constructs

We investigated the possibility of producing 3D dentin–pulp complexes with patient-specific shapes by utilizing the 3D hybrid bioprinting process.[26] Polycaprolactone (PCL; Polysciences Inc., Warrington, PA, USA) was used

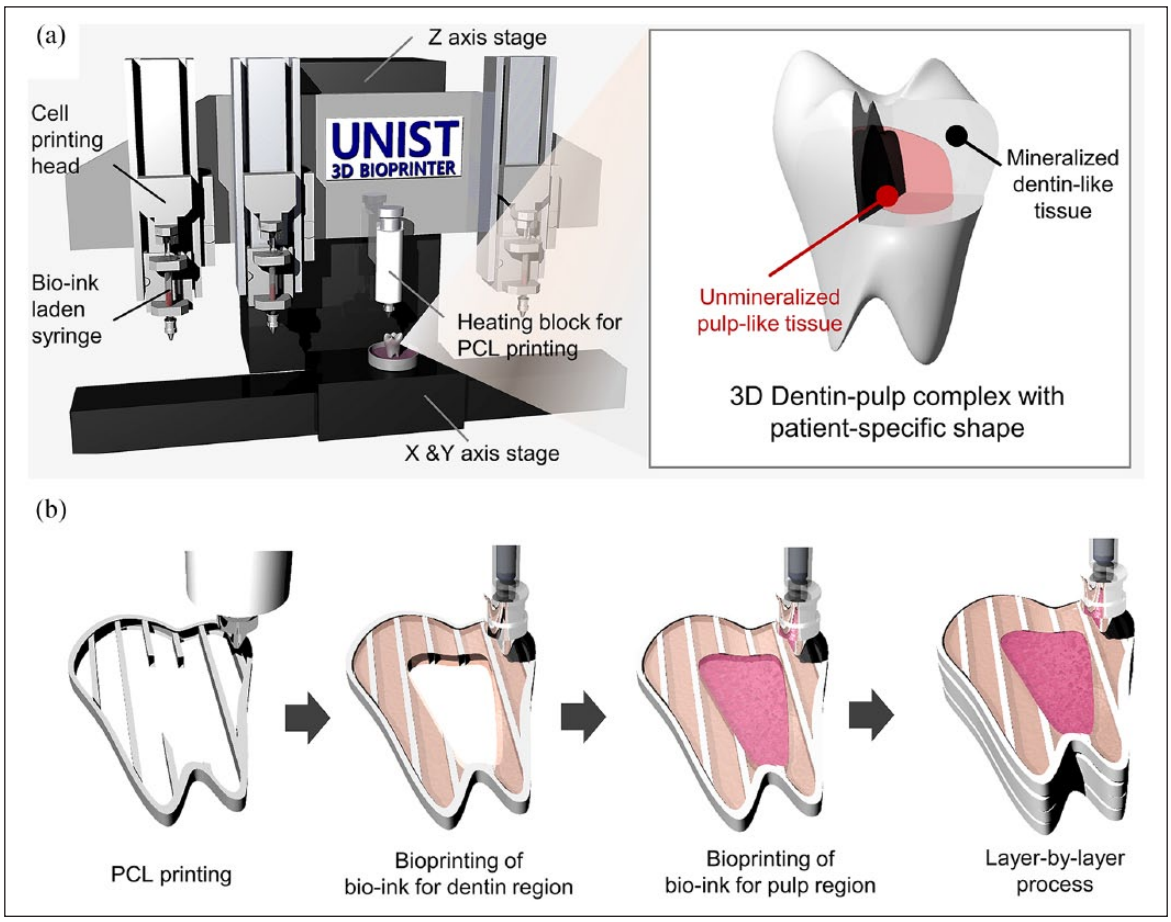

Figure 1. Bioprinting process of patient-specific shaped 3D dentin–pulp complexes. The illustrations show schematic drawings of the (a) 3D bioprinter and (b) printing process to produce patient-specific shaped 3D dentin–pulp complexes. The complex was constructed by serial printing of PCL and two bio-inks for dentin and pulp tissue in a layer-by-layer manner.

to reproduce 3D overall shape of the tooth and two types of bio-inks (F5- and F20-bio-ink) were used to simulate dentin–pulp complexes (Figure 1(b)). The process began by imaging a human tooth with micro-computed tomography (CT), and the data were then converted to a 3D computer-aided design (CAD) model (STL format).[24,27] The CAD model was loaded into an in-house computer-aided manufacturing (CAM) software package to obtain a motion program, and the printing process was performed by applying the program to a bioprinter. Figure 1(b) shows this printing process. After melting PCL at 90°C with a syringe heating block, PCL was printed first with 300-μm metal nozzle to fabricate the outline of the patient-specific tooth by applying 780 kPa pressure. The hDPSC-laden F20- and F5-bio-inks were then applied for printing of dentin and pulp tissue through 250-μm nozzle using mechanical dispenser system, respectively. PCL was selected as scaffold component due to their 3D printable properties, proper mechanical properties for maintaining overall shape during culture, long-term biodegradability, biocompatibility, and affinity for hard tissue (including pulp–dentin tissue) regeneration.[28,29] The 3D cellular construct was produced through repetition of this process with stacking as shown in Figure 1(b). In printing processes, the enclosure was maintained at 18°C. After printing, the construct was crosslinked with thrombin (10 U/mL) (Sigma) solution at room temperature for 45 min and cultured with odontogenic differentiation medium.

Characterization of bio-ink

Scanning electron microscopy (SEM; S-4800; Hitachi High-Technologies Co., Tokyo, Japan) was used to investigate the micro-architecture of the crosslinked bio-ink, recorded at 5.0 kV. The compressive modulus and rheological properties of the fibrin-based bio-inks were measured with a mechanical testing machine (Instron Model 3342; Illinois Tool Works Inc., Norwood, MA, USA) and a sliding plate rheometer (HAAKE MARS III Rheometer; Thermo Scientific, Karlsruhe, DE, Germany), respectively. For in vitro degradation tests, hDPSC-laden bio-inks (3×10^6 cells/mL) were loaded in a 24-well plate and then crosslinked. After 5 days of cultivation with growth medium, the wet weight of the bio-inks was measured and normalized relative to the data from day 1.

Cytocompatibility

Live and dead staining (L3224; Thermo Fisher Scientific, Waltham, MA, USA) was performed in order to measure the viability of the bioprinted hDPSCs. The samples were stained with assay solution (0.2% v/v calcein AM and 0.05% v/v ethidium homodimer-1 in phosphate-buffered saline (PBS)) at room temperature for 45 min and then imaged using a fluorescent microscope (Leica DM2500; Leica Microsystems AG, Wetzlar, Germany). The live and dead cells were manually counted and the cell viability was calculated by dividing the number of live cells by the total cell count.

Proliferation was evaluated using alamarBlue™ Cell Viability Reagent (ThermoFisher Scientific). The samples cultured for 1, 3, and 5 days were incubated in 10% v/v alamar blue dye diluted by growth medium at 37°C and 5% CO_2 for 3 h. After sampling the assay solutions in 100-μL aliquots, their fluorescence intensities (excitation: 544 nm/emission: 599 nm) were measured with a microplate reader (Synergy NEO2 Hybrid Multi-Mode Reader; Bio-Tek, Winooski, VT, USA). The measured data were normalized relative to the data collected on day 1.

Identification of odontogenic differentiation

Alizarin red S staining was performed to confirm mineral deposition. Samples fixed with 4% paraformaldehyde (PFA) solution were stained with an alizarin red S (Sigma) solution of 2% w/v diluted by 2DW at pH 4.3 for 20 min. To quantify the mineral deposition, the stained samples were de-stained with 10% cetylpyridinium chloride solution in 10 mM sodium phosphate buffer (pH 7.0) overnight. The optical density of each de-stained sample was measured utilizing a microplate reader at 550 nm.

The messenger RNA (mRNA) expression of dentin matrix acid phosphoprotein 1 (DMP-1) and dentin sialophosphoprotein (DSPP) in each sample was quantitatively evaluated. For RNA extraction, each sample was treated with Trisure (Bioline, London, UK) for 10 min. The extracted RNA was used for complementary DNA (cDNA) synthesis using HelixCript™ Thermo Reverse Transcriptase (NanoHelix, Daejeon, South Korea). Biometra TProfessional TRIO Thermo-cycler (Analytik Jena AG, Jena, Germany) was used for the synthesis. The cDNA mixed with appropriate primers (Supplemental Appendix Table 1) was amplified with Roche SYBR Light Cycler 480 SYBR Green I Master (Roche Diagnostics Gmbh, Mannhein, Germany) using a light cycler 480 II (Roche Diagnostics GmbH). Expression levels of DMP-1 and DSPP were normalized to glyceraldehyde 3-phosphate dehydrogenase (GAPDH) via the ΔΔCt method.

Statistical analysis

All variables are expressed as means ± standard error of the mean (SE). Statistical analyses were performed using Excel (Microsoft Corp., Redmond, WA, USA). Multiple comparisons between experimental groups were conducted by one-way analysis of variance (ANOVA) and Tukey's multiple comparison test. Before analysis, the equality of variance was assessed using statistical analysis software (Version 19.0; IBM SPSS, Chicago, IL, USA) to evaluate whether the use of Tukey's multiple comparison test is appropriate. In all analyses, $p < 0.05$ was taken to indicate statistical significance.

Results

Fibrin-based bio-ink and its hDPSC compatibility

Physical properties of the prepared bio-inks were investigated. Figure 2(a) and (b) shows SEM images and measured compressive modulus of the crosslinked bio-inks. As shown, the crosslinked bio-ink had a pore size of 2–4 μm. The pore size, measured by SEM, decreased with increasing fibrinogen concentration and the F20-bio-ink had an average pore size of 2.2 μm, which is similar to that of a human dentinal tubule (~2.5 μm pores) (Supplemental Appendix Figure 1). The compressive modulus increased with increasing fibrinogen concentration within the bio-ink (Figure 2(b)). The compressive modulus of the bio-ink increased approximately 1.5 times as the fibrinogen concentration increased from 5 to 20 mg/mL. The fibrinogen concentration also affected the degradation properties of the bio-ink (Figure 2(c)). The degradation rate decreased with increasing concentration of fibrinogen, and the degradation rate of F20-bio-ink was half that of the F5-bio-ink.

Figure 2(d)–(f) shows test results of hDPSC compatibility of the designed bio-inks. The overall finding was that the designed fibrin-based bio-ink is quite feasible for hDPSC printing and culturing. Figure 2(d) shows the viability of hDPSCs within bio-inks. On the day 4 of culturing, cell viability was >90% in all groups. Continued proliferation of cells in growth medium was observed for 16 days (Figure 2(e)). The proliferation rate of hDPSC decreased with increasing fibrinogen concentration. Figure 2(f) shows the change in morphology of hDPSC within bio-ink during the culturing. The higher the fibrinogen concentration, the longer the time required to show the stretched morphology of the cell; all groups showed similar stretched morphologies after day 4.

Printability of fibrin-based bio-ink

Viscosity and printability of the designed fibrin-based bio-ink were investigated. Figure 3(a) shows the rheology test results of the bio-inks. As shown, the viscosity of bio-ink increased with increasing fibrinogen concentration. On the other hand, the variation of fibrinogen concentration did not affect the shear thinning properties of the bio-inks, a property which was well maintained in all groups. The change in viscosity of bio-ink affected the printing results. Figure 3(b) shows measured line widths printed with the bio-inks,

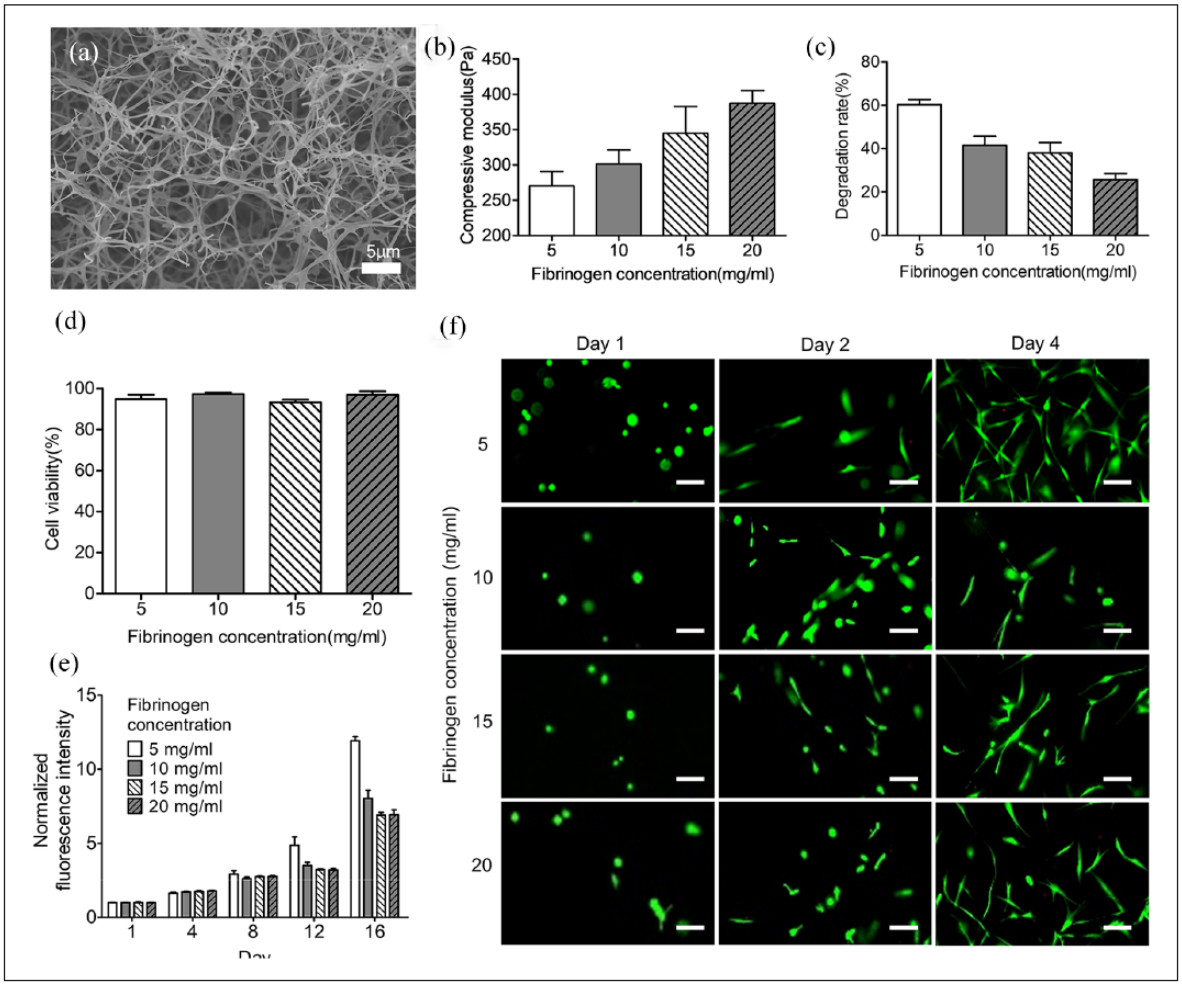

Figure 2. Properties of fibrin-based bio-inks: (a) Scanning electron microscopic image of a crosslinked F20-bio-ink, showing a pore size of approximately 2.2 μm. (b) Compressive modulus of bio-inks with variation in fibrinogen concentration (n = 3). (c) Measured degradation rates of bio-inks on day 5 (n = 3). (d) Cell viability assay results of hDPSC-laden bio-inks after culturing for 4 days (n = 6). (e) Proliferation rate of hDPSC within bio-ink for 16 days. Metabolic activity was measured with alamarBlue™ assay solution and normalized relative to the data from day 1 (n = 5). (f) Fluorescence image of live cell–stained samples after culturing for 4 days (scale bars: 50 μm). Live cells are shown in green. Each bar in the graphs represents the mean ± SE.

demonstrating that the line width tended to slightly decrease with increasing fibrinogen concentration. However, no statistical significance was observed between F5- and F15-bio-ink groups, and the printed minimum line width in this test was approximately 160 μm. We also examined the effect of printing speed on the patterning results (Figure 3(c)). As the printing speed increased, the line width gradually decreased. Greater variation of line width was observed at lower concentrations of fibrinogen. Based on these results, micro-patterns with hDPSC can be achieved and controlled by adjusting printing speed and fibrinogen concentration.

We printed the word "UNIST" with hDPSC-laden bio-ink to verify its performance for freeform patterning (Figure 3(d)). Living hDPSCs are shown in green. As shown, a designed micro-pattern with 200-μm line widths was well-fabricated with the designed bio-ink. Figure 3(e) shows viability test results of the printed hDPSCs, with non-printed hDPSCs used as a control group. As shown here, the control and printed groups showed similar cell viabilities (>88% on day 1). In the proliferation test, activated proliferation of cells was observed in both groups for 5 days (Figure 3(f)). These results confirmed that the designed bio-ink and bioprinting process in this study are quite feasible for freeform patterning with living hDPSCs.

Spatial regulation of hDPSC differentiation within bioprinted constructs

We examined the possibility of spatial regulation of hDPSC differentiation with bioprinting techniques. Here, the effect of fibrinogen concentration in odontogenic differentiation of hDPSC was investigated. As a result of alizarin red S staining, mineral deposition increased significantly as fibrinogen concentration of the bio-ink

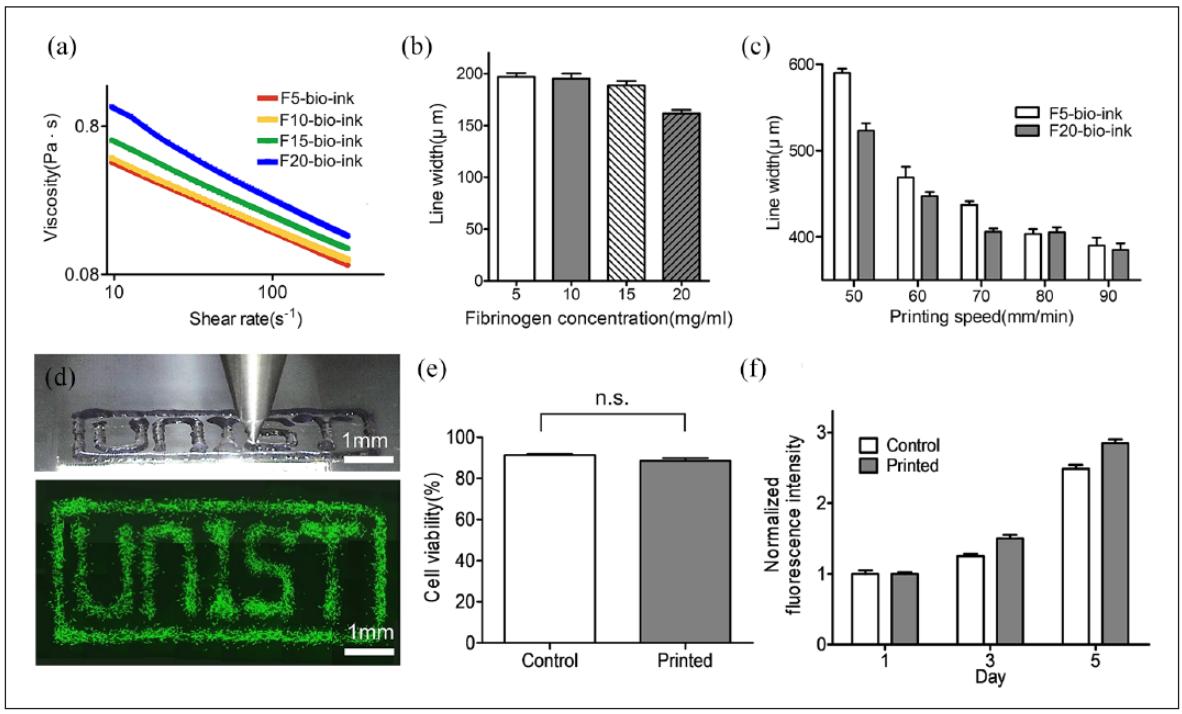

Figure 3. Printability of fibrin-based bio-ink. (a) Rheological properties of the prepared bio-inks. (b) Measured width of live pattern printed with the fibrin-based bio-ink with variable fibrinogen concentration. The line patterns were printed with a 100-μm nozzle, printing speed of 140 mm/min and dispensing rate of 34.55 nL/s (n = 10). (c) Bioprinted line width with variation in printing speed from 50–90 mm/min. A nozzle size of 200 μm, dispensing rate of 138.21 nL/s, and F5- and F20-bio-ink were used in this experiment (n = 10). (d) Microscope (upper) and fluorescence (lower) image showing "UNIST" printed with hDPSC-laden bio-ink. Cells were stained with calcein AM to identify live cells (in green). (e) Viability of bioprinted hDPSC in fibrin-based bio-inks after culturing for 1 day. Non-bioprinted hDPSC-laden bio-inks were used as a control group (n = 4). (f) Proliferation rate of printed and non-printed (control) bio-inks. Metabolic activity was measured with alamarBlue™ assay solution and normalized relative to the data from day 1 (n = 4). Each bar in the graphs represents the mean ± SE. *$p < 0.05$.

increased (Figure 4(a)). Any evidence for mineral deposition was not observed in the F5-bio-ink group, although it was cultured with differentiation medium. The group showed similar OD (optical density) values as the undifferentiated control group which was cultured with growth medium. This tendency was also observed during gene expression (Figure 4(b)). As a result of quantitative reverse transcription polymerase chain reaction (RT-qPCR), expression of DMP1 and DSPP, the major markers of odontogenic differentiation of hDPSC, increased with fibrinogen concentration. The F5-bio-ink group showed a similar expression level as the undifferentiated control group.

Figure 4(c) shows a microscopy image depicting hDPSC morphology within the F20-bio-ink. As shown, hDPSCs in the bio-ink maintained the polarized morphology of odontoblasts even after 25 days of cultivation.[30] Calcium phosphate crystals, which are observed mainly in the mineral deposition of hDPSCs, were also observed (Supplemental Appendix Figure 2).[31] Based on the mineral deposition results, odontogenic gene expression, odontoblast-like morphology, and mineral crystals with specific shapes, the fate of hDPSCs can be regulated by controlling the fibrinogen concentration of the bio-ink.

Based on these results, we performed two-dimensional (2D) patterning with both F5- and F20-bio-inks. Figure 4(d) shows staining results with calcein AM on the printed pattern, where the green color shows living hDPSCs. As shown here, the population of printed hDPSCs was dense in the outer region and sparse in the center region reminiscent of cell-rich and cell-free zone of pulp tissue, respectively.[32] However, hDPSC alignment was not observed in this experiment. Figure 4(e) shows the alizarin red S staining results of the samples cultured with differentiation media for 15 days. As shown, locally concentrated mineral depositions were successfully achieved similar to dentin–pulp complex.

Bioprinting of 3D dentin–pulp complexes with human tooth shapes and sizes

The 3D bioprinting was applied to produce a patient-specific shaped 3D composite tissue for tooth regeneration. Figure 5(a) shows the transforming procedure

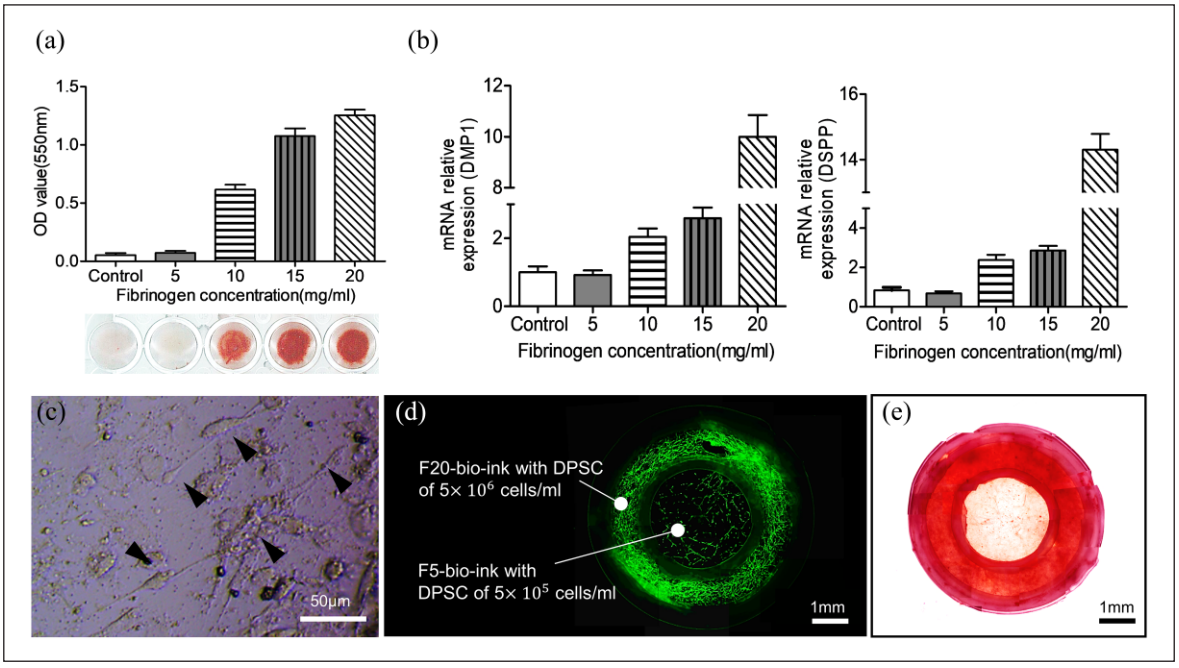

Figure 4. Spatial regulation of odontogenic differentiation of hDPSC. (a) Alizarin red S staining result of hDPSC-laden bio-inks with four different concentrations of fibrinogen, which were cultured with differentiation medium for 15 days. Photograph and graph show the stained samples and optical density of de-stained solution of the samples, respectively (n = 4). (b) Odontogenic gene expression of hDPSC within the bio-inks after culturing with differentiation medium. After measuring with RT-qPCR, DSPP and DMP-1 level were normalized relative to the data of the control group. hDPSC in F5-bio-ink cultured with growth medium was used as an un-differentiated control (n = 7). (c) Optical microscopy image showing hDPSC morphology within bio-ink after culturing with differentiation medium for 25 days. (d) Fluorescence image showing a 2D patterned sample with two types of bio-ink, F5- and F20-bio-ink. The sample was stained with calcein AM to identify live cells (in green). (e) Optical microscopy image showing alizarin red S staining result of the 2D patterned sample after culturing with differentiation medium for 15 days. Each data point represents the mean ± SE.

from CAD model to printing code, which was processed with homemade CAM software. Figure 5(b) and (c) shows CAD model and printing results for a human tooth approximately 8 mm × 8 mm × 20 mm in size, respectively. As shown, the 3D bioprinting process is quite feasible for fabricating a cellular structure similar in shape and size with a human tooth. Figure 5(d) shows alizarin red S staining results for the horizontal cross section of the printed 3D construct. As with the 2D printing results (Figure 4(e)), mineral deposition was locally observed only in the outer region, and not in the center region of the pulp tissue. This result confirmed that the designed 3D bioprinting process could induce localized odontogenic differentiation in a designed 3D space, specifically patient-specific shaped 3D dentin–pulp complexes.

Discussion

In this study, fibrin-based bio-ink was designed for 3D printing with hDPSCs. Fibrin gel, a main component of bio-ink, is a biopolymer derived from blood and suitable for cell adhesion, with good mass transfer of oxygen and nutrients.[33–35] In addition, it can be directly extracted from the patient's blood, which is advantageous in terms of avoiding immune reactions in clinics.[36] Several studies have reported that fibrin gel provides an excellent biological environment for culturing tooth cells. In this study, the designed fibrin-based bio-ink showed good hDPSC compatibility in terms of viability and proliferation. hDPSC morphology was well-maintained after 25-day long-term culture (Figures 2(d)–(f) and 4(c)). In addition, this bio-ink showed excellent printability in that micro-patterning up to 160 μm was possible without cell damage. Thus, the designed fibrin-based bio-ink met the key requirements for 3D bioprinting in terms of cytocompatibility and printability.

In tooth tissue engineering, patient-specific shape is a key factor for clinical applications. Size and shape mismatching can cause various problems such as facial asymmetry, language pronunciation, and impaired mastication.[37–39] This study applied CT data to the bioprinting, which was converted to printing code. The result successfully demonstrated that the designed bio-ink and 3D hybrid bioprinting could produce 3D patient-specific cellular constructs for tooth tissue engineering in a pre-defined manner.

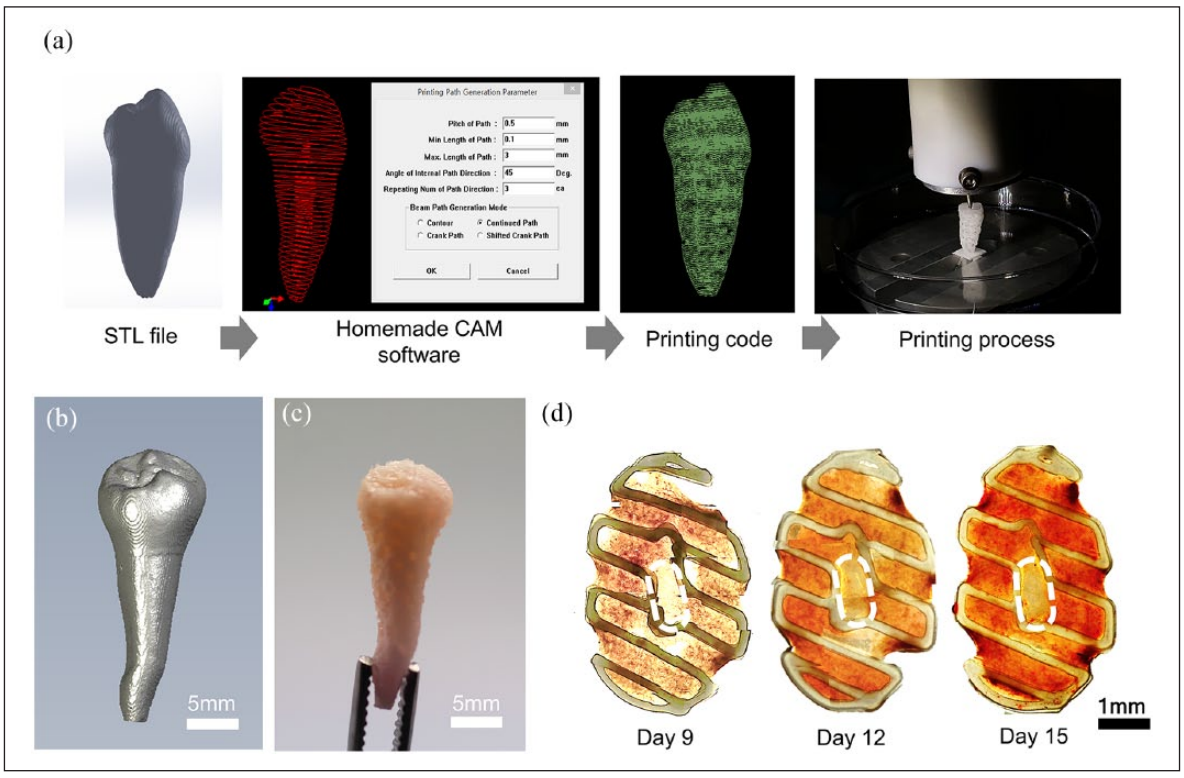

Figure 5. Bioprinting of patient-specific shaped 3D dentin–pulp complex with localized mineralization. (a) Flow chart of the overall process from CAD model to printing. Printing code for dental composite tissue was converted from CAD model of STL format using in-house CAM software and was applied to the bioprinter to construct the designed cellular structure. (b) Measured micro-CT image of a real human tooth. (c) Bio-printed 3D dentin–pulp complex with patient-specific shape. (d) Alizarin red S staining results of sliced cross section of the dentin–pulp complex. The white color dotted circle shows the central, un-mineralized area for pulp region.

In dentin–pulp complexes, hDPSCs are present as mesenchymal stem cells in pulp tissue at the center of the tooth, and dentin tissue at the outer region is composed of mineralized extracellular matrix (ECM) supported by differentiated odontoblastic layer. Therefore, it is important to spatially control the odontogenic differentiation of hDPSCs within a 3D dentin–pulp complex. According to this study, the differentiation of hDPSCs was affected by the fibrinogen concentration, because the physical properties of the bio-ink (such as the stiffness and the diffusion coefficient) varied according to the concentration. Among them, stiffness was considered as a major cause of these differences, as other studies have previously reported.[40,41] Based on the experiment results, we selected two bio-inks, F5- and F20-bio-ink, for spatial control of odontogenic differentiation of hDPSCs for the production of dentin–pulp complexes. By applying the bio-inks to bioprinting, the outer dentin region of the printed 3D construct promoted active odontogenic differentiation. On the other hand, the central pulp region was well-maintained as undifferentiated. Localized mineral deposition in the outer region was also observed (Figures 4(e) and 5(d)). This result successfully demonstrated that the spatial regulation of hDPSC differentiation for the production of 3D dentin–pulp complexes can be realized using designed bio-inks and bioprinting process. In future studies, the printing process for surrounding tissues including cementum and periodontal ligament tissue will be developed to regenerate a whole tooth. A study on the strengthening of artificial teeth using ceramics and other high strength biomaterials will be also carried out.

Acknowledgements

The authors are thankful to Dr Jin Man Kim of CHA University School of Medicine for his help in preparing this paper.

Declaration of conflicting interests

The author(s) declared no potential conflicts of interest with respect to the research, authorship, and/or publication of this article.

Funding

The author(s) disclosed receipt of the following financial support for the research, authorship, and/or publication of this article: This work was supported by the Bio & Medical Technology Development Program (NRF-2017M3A9E4047243) funded by the Ministry of Science, ICT and Future Planning, Republic of Korea.

Supplemental material

Supplemental material for this article is available online.

ORCID iD

Hyung-Ryong Kim https://orcid.org/0000-0002-6710-6964

References

1. Dye BA, Thornton-Evans G, Li X, et al. *Dental caries and tooth loss in adults in the United States, 2011–2012*. Hyattsville, MD: National Center for Health Statistics, 2015.
2. Vos T, Flaxman AD, Naghavi M, et al. Years lived with disability (YLDs) for 1160 sequelae of 289 diseases and injuries 1990–2010: a systematic analysis for the Global Burden of Disease Study 2010. *Lancet* 2012; 380(9859): 2163–2196.
3. Greenstein G, Cavallaro J, Romanos G, et al. Clinical recommendations for avoiding and managing surgical complications associated with implant dentistry: a review. *J Periodontol* 2008; 79(8): 1317–1329.
4. Jung RE, Pjetursson BE, Glauser R, et al. A systematic review of the 5-year survival and complication rates of implant-supported single crowns. *Clin Oral Implants Res* 2008; 19(2): 119–130.
5. Cassetta M, Pranno N, Calasso S, et al. Early peri-implant bone loss: a prospective cohort study. *Int J Oral Maxillofac Surg* 2015; 44(9): 1138–1145.
6. Nakao K, Morita R, Saji Y, et al. The development of a bioengineered organ germ method. *Nat Methods* 2007; 4(3): 227–230.
7. Oshima M, Mizuno M, Imamura A, et al. Functional tooth regeneration using a bioengineered tooth unit as a mature organ replacement regenerative therapy. *PLoS ONE* 2011; 6(7): e21531.
8. Zhang W, Abukawa H, Troulis MJ, et al. Tissue engineered hybrid tooth-bone constructs. *Methods* 2009; 47(2): 122–128.
9. Young CS, Terada S, Vacanti JP, et al. Tissue engineering of complex tooth structures on biodegradable polymer scaffolds. *J Dent Res* 2002; 81(10): 695–700.
10. Yelick PC and Vacanti JP. Bioengineered teeth from tooth bud cells. *Dent Clin North Am* 2006; 50(2): 191–203.
11. Honda MJ, Tsuchiya S, Sumita Y, et al. The sequential seeding of epithelial and mesenchymal cells for tissue-engineered tooth regeneration. *Biomaterials* 2007; 28(4): 680–689.
12. Duailibi SE, Duailibi MT, Zhang W, et al. Bioengineered dental tissues grown in the rat jaw. *J Dent Res* 2008; 87(8): 745–750.
13. Ono M, Oshima M, Ogawa M, et al. Practical whole-tooth restoration utilizing autologous bioengineered tooth germ transplantation in a postnatal canine model. *Sci Rep* 2017; 7: 44522.
14. Yang JW, Zhang YF, Sun ZY, et al. Dental pulp tissue engineering with bFGF-incorporated silk fibroin scaffolds. *J Biomater Appl* 2015; 30(2): 221–229.
15. AbdulQader ST, Kannan TP, Rahman IA, et al. Effect of different calcium phosphate scaffold ratios on odontogenic differentiation of human dental pulp cells. *Mater Sci Eng C Mater Biol Appl* 2015; 49: 225–233.
16. Smith EE, Zhang W, Schiele NR, et al. Developing a biomimetic tooth bud model. *J Tissue Eng Regen Med* 2017; 11(12): 3326–3336.
17. Leyendecker Junior A, Gomes Pinheiro CC, Lazzaretti Fernandes T, et al. The use of human dental pulp stem cells for in vivo bone tissue engineering: a systematic review. *J Tissue Eng*. Epub ahead of print 17 January 2018. DOI: 10.1177/2041731417752766.
18. Chalisserry EP, Nam SY, Park SH, et al. Therapeutic potential of dental stem cells. *J Tissue Eng*. Epub ahead of print 23 May 2017. DOI: 10.1177/2041731417702531.
19. Murphy SV and Atala A. 3D bioprinting of tissues and organs. *Nat Biotechnol* 2014; 32(8): 773–785.
20. Langton CM, AlQahtani SM and Wille M-L. A 3D-printed passive ultrasound phase-interference compensator for reduced wave degradation in cancellous bone—an experimental study in replica models. *J Tissue Eng*. Epub ahead of print 1 April 2018. DOI: 10.1177/2041731418766418.
21. Ludwig PE, Huff TJ and Zuniga JM. The potential role of bioengineering and three-dimensional printing in curing global corneal blindness. *J Tissue Eng*. Epub ahead of print 13 April 2018. DOI: 10.1177/2041731418769863.
22. Kolesky DB, Truby RL, Gladman AS, et al. 3D bioprinting of vascularized, heterogeneous cell-laden tissue constructs. *Adv Mater* 2014; 26(19): 3124–3130.
23. Jung JW, Lee JS and Cho DW. Computer-aided multiple-head 3D printing system for printing of heterogeneous organ/tissue constructs. *Sci Rep* 2016; 6: 21685.
24. Kang HW, Park JH, Kang TY, et al. Unit cell-based computer-aided manufacturing system for tissue engineering. *Biofabrication* 2012; 4(1): 015005.
25. Obregon F, Vaquette C, Ivanovski S, et al. Three-dimensional bioprinting for regenerative dentistry and craniofacial tissue engineering. *J Dent Res* 2015; 94(9 Suppl.): 143S–152S.
26. Kang HW, Lee SJ, Ko IK, et al. A 3D bioprinting system to produce human-scale tissue constructs with structural integrity. *Nat Biotechnol* 2016; 34(3): 312–319.
27. Lim S-H, Kim M-K and Kang S-H. Genioplasty using a simple CAD/CAM (computer-aided design and computer-aided manufacturing) surgical guide. *Maxillofac Plast Reconstr Surg* 2015; 37(1): 44.
28. Heo S-Y, Ko S-C, Oh G-W, et al. Fabrication and characterization of the 3D-printed polycaprolactone/fish bone extract scaffolds for bone tissue regeneration. *J Biomed Mater Res B Appl Biomater*. Epub ahead of 3 December 2018. DOI: 10.1002/jbm.b.34286.
29. Ma Y, Xie L, Yang B, et al. Three-dimensional printing biotechnology for the regeneration of the tooth and tooth-supporting tissues. *Biotechnol Bioeng* 2019; 116(2): 452–468.
30. Arana-Chavez VE and Massa LF. Odontoblasts: the cells forming and maintaining dentine. *Int J Biochem Cell Biol* 2004; 36(8): 1367–1373.
31. Potdar PD and Jethmalani YD. Human dental pulp stem cells: applications in future regenerative medicine. *World J Stem Cells* 2015; 7(5): 839–851.
32. Modena KC, Casas-Apayco LC, Atta MT, et al. Cytotoxicity and biocompatibility of direct and indirect pulp capping materials. *J Appl Oral Sci* 2009; 17(6): 544–554.
33. Lee J-H and Kim H-W. Emerging properties of hydrogels in tissue engineering. *J Tissue Eng*. Epub ahead of 29 March 2018. DOI: 10.1177/2041731418768285.

34. Jin G-Z and Kim H-W. Efficacy of collagen and alginate hydrogels for the prevention of rat chondrocyte dedifferentiation. *J Tissue Eng*. Epub ahead of 8 October 2018. DOI: 10.1177/2041731418802438.
35. Dashnyam K, Lee J-H, Mandakhbayar N, et al. Intra-articular biomaterials-assisted delivery to treat temporomandibular joint disorders. *J Tissue Eng*. Epub ahead of 13 May 2018. DOI: 10.1177/2041731418776514.
36. Galler KM, Cavender AC, Koeklue U, et al. Bioengineering of dental stem cells in a PEGylated fibrin gel. *Regen Med* 2011; 6(2): 191–200.
37. Barone S, Neri P, Paoli A, et al. Design and manufacturing of patient-specific orthodontic appliances by computer-aided engineering techniques. *Proc Inst Mech Eng H* 2018; 232(1): 54–66.
38. Thilander B, Pena L, Infante C, et al. Prevalence of malocclusion and orthodontic treatment need in children and adolescents in Bogota, Colombia. An epidemiological study related to different stages of dental development. *Eur J Orthod* 2001; 23(2): 153–167.
39. Yamaguchi H and Sueishi K. Malocclusion associated with abnormal posture. *Bull Tokyo Dent Coll* 2003; 44(2): 43–54.
40. Her GJ, Wu HC, Chen MH, et al. Control of three-dimensional substrate stiffness to manipulate mesenchymal stem cell fate toward neuronal or glial lineages. *Acta Biomater* 2013; 9(2): 5170–5180.
41. Singh M, Dormer N, Salash JR, et al. Three-dimensional macroscopic scaffolds with a gradient in stiffness for functional regeneration of interfacial tissues. *J Biomed Mater Res A* 2010; 94(3): 870–876.